AIP | Applied Physics Letters

Origins of nanostructure in amorphous polymer coatings via matrix assisted pulsed laser evaporation

Kimberly B. Shepard, Craig B. Arnold, and Rodney D. Priestley

Citation: Appl. Phys. Lett. **103**, 123105 (2013); doi: 10.1063/1.4821366
View online: http://dx.doi.org/10.1063/1.4821366
View Table of Contents: http://apl.aip.org/resource/1/APPLAB/v103/i12
Published by the AIP Publishing LLC.

Origins of nanostructure in amorphous polymer coatings via matrix assisted pulsed laser evaporation

Kimberly B. Shepard,[1] Craig B. Arnold,[2,3] and Rodney D. Priestley[1,3,a)]
[1]*Department of Chemical and Biological Engineering, School of Engineering and Applied Sciences, Princeton University, Princeton, New Jersey 08544, USA*
[2]*Department of Mechanical and Aerospace Engineering, School of Engineering and Applied Sciences, Princeton University, Princeton, New Jersey 08544, USA*
[3]*Princeton Institute for the Science and Technology of Materials, Princeton University, Princeton, New Jersey 08544, USA*

(Received 4 July 2013; accepted 30 August 2013; published online 17 September 2013)

We investigate the nanostructure of sub-monolayer and monolayer amorphous polymer films deposited via Matrix Assisted Pulsed Laser Evaporation (MAPLE). The structure is quantified by analyzing the size distribution of polymer nanoglobules as a function of deposition parameters: time and polymer concentration. Two deposition regimes are observed in the early stages of MAPLE deposition, with a transition at a critical time. The observed distribution of nanoglobule sizes that is present after the critical time agrees well with prior molecular dynamics simulations of the MAPLE process. We discuss the mechanism of nanostructured coatings within the framework of the Zhigilei model. © *2013 AIP Publishing LLC*. [http://dx.doi.org/10.1063/1.4821366]

Matrix Assisted Pulsed Laser Evaporation (MAPLE) is a laser-ablation thin film deposition technique in which thin films of the desired material are deposited from a frozen dilute solution. MAPLE has been successfully shown to deposit a wide array of polymeric materials, including poly(methyl methacrylate) (PMMA), polysiloxane, polythiophene, poly (ethylene glycol), polyisobutylene, polyethylenimine, and polyfluorene.[1,2] As a route for thin film deposition, MAPLE has numerous advantages over more conventional approaches, including spin casting. In particular, MAPLE enables precise film thickness control coupled with the ability to deposit more complex structures, including multilayer[3] and patterned[4] films at controlled growth rates. Targeted applications that are anticipated to benefit from the deposition capabilities of MAPLE include organic electronics,[5,6] coatings for medical implants and drug delivery,[7,8] and sensors.[9,10]

Recent reports of nanostructured MAPLE films[11–13] have raised questions about the origins of nanoscale assembly in the deposited materials. The formation of nanostructure in polymer films via MAPLE may occur during two distinct stages of the deposition process. In one case, the film may become nanostructured subsequent to material deposition by a mechanism, such as evaporation-induced self assembly, where directional evaporation of the solvent causes 2D ordering in the deposited film.[12] In the second case, structure is set-in prior to the deposition of the desired material atop the substrate. That is, self-assembly of the nanoscale structures occurs within the time frame of the transfer process between the target and substrate.[11] In this work, we are concerned with the latter mechanism of nanostructured film formation.

In prior work, we have demonstrated that thin films of PMMA prepared by MAPLE may exhibit a nanostructured geometry, which is formed by the assembly of intact nanoglobules.[14] Atomic Force Microscope (AFM) topological imaging revealed the presence of surface nanoglobules, while cross-sectional Scanning Electron Microscope (SEM) imaging revealed their presence throughout the entire coating.[14] In comparison to spin cast PMMA coatings, in which no structure is present, coatings prepared by MAPLE exhibited improved thermal and kinetic stability.[14] For instance, the glass transition temperature (T_g) of the films was enhanced by 40 K, the increase of which would facilitate greater application of the films as coatings in high temperature environments. The improved material properties have been postulated to result from the nanostructure, and a recent study provides a connection between the film structure and property enhancements.[11] Nevertheless, how the structure is formed may be just as important as the structure itself in leading to the unique material properties. Thus, the origins of nanostructure formation in MAPLE-deposited films should be pursued not only as a means of providing guidance for tuning material properties of coatings but also for elucidating greater fundamental understanding of the deposition process.

In order to understand the origins of nanostructured films in the MAPLE process, this study investigates the structure of sub-monolayer and monolayer coatings of PMMA deposited atop silicon oxide substrates. These experiments entail characterizing, both visually and quantitatively, the nanostructure, i.e., nanoglobule morphology of isolated nanoglobules and monolayer films as a function of deposition time. We also characterize the influence of polymer target concentration on the nanostructure morphology during the early stages of film growth. By performing these measurements, we provide insight into the mechanism of nanostructured film formation, in which polymer/solvent clusters ejected by the laser self-assemble into the polymer nanoglobules which compose the film.

PMMA ($M_w = 14\,100$ g/mol by Gel Permeation Chromatography, Polydispersity Index = 1.85) from Sigma Aldrich was used as-received. Previous work[14] has demonstrated that this polymer is amorphous after MAPLE deposition. PMMA was dissolved in as-received chloroform

a)Author to whom correspondence should be addressed. Electronic mail: rpriestl@princeton.edu

(99.9%, Acros Organics) at percentages of 0.05%, 0.1%, 0.5%, and 1% by weight for use as the target solution for MAPLE deposition. Approximately 10 ml of the target solution was frozen in a liquid nitrogen reservoir and maintained at low temperature (~120 K) inside the MAPLE chamber. During deposition, the chamber pressure was maintained at $\sim 10^{-4}$ Torr. The target was ablated by a pulsed excimer laser (LightMachinery PulseMaster 844, $\lambda = 248$ nm, pulse duration = 20 ns, 5 Hz repetition rate, ~ 0.125 J/cm^2 fluence and ~ 15 mm^2 spot area) at an angle of 45°. The ablated material was deposited onto silicon oxide substrates held at a constant temperature of 300 K ($\sim 0.85 T_g$ of PMMA, $T_g = 355$ K). Low degassing thermal paste was used to ensure uniform heat transfer from the heated substrate to the silicon oxide slides.

Deposited films were characterized using a Veeco Dimension V Nanoman AFM. All images shown here are phase images and are 2 × 2 μm in size. AFM image processing and analysis were performed using Gwyddion[15] and ImageJ[16] software, respectively. More specifically, ImageJ software was used to calculate the two-dimensional projected area occupied by each nanoglobule of a deposited film. Radii were calculated by assuming that the globules were circular in shape. The volume of the globules was estimated using a spherical cap geometry, in which the globule height was measured to be approximately 1/3 of the footprint radius. The number of mers (monomer units in a polymer chain) in a globule of given radius (R) was calculated, assuming a radius of gyration (R_g) of 2 nm and 100 mers per polymer chain.

To isolate the early-time MAPLE deposition behavior, we investigated the effect of MAPLE deposition time on the nanostructure of the deposited films. Five deposition times were examined (2.5, 5, 10, 20, and 40 min), while maintaining a constant polymer concentration of 0.1% by weight. AFM phase images for three of the resulting depositions (2.5, 10, and 40 min) are shown in Figure 1. The shortest deposition time (see Fig. 1(a)) yielded small, isolated nanoglobules distributed atop the silicon oxide substrate. The substrate was abraded with a razor to confirm the absence of an underlying planar layer. The individual nanoglobules resemble wetted droplets, whose geometry can be approximated as a spherical cap. The globules occupy approximately 16% of the substrate area, and the substrate is visible between the globules. After 10 min of MAPLE deposition, a near-continuous polymer film was formed, consisting of a monolayer of nanoglobules with minimal overlap (see Fig. 1(b)). In this deposition, a small number of globules were deposited on top of other globules, and the substrate was visible only in small discontinuities in the film. This 10 min deposition demonstrated a nanostructured polymer film with an average thickness of just 40 nm. For a deposition time of 40 min, the substrate was covered fully, and more overlapping of nanoglobules was observed (see Fig. 1(c)). To better quantify the differences in film nanostructure, we used image analysis software to measure the size distributions of the nanoglobules. We note that for depositions with times ≥5 min, an ultrathin planar film 2–5 nm in thickness was present between the substrate and nanoglobules.

Figure 1(d) is a histogram plot of the nanoglobule size distribution for the five different MAPLE deposition times. The size distributions for the two shortest deposition times, 2.5 and 5 min, were similar, with a narrow breadth (FWHM = 11 and 13 nm, respectively) and a peak at 20 nm. The three longer deposition times (10, 20, and 40 min) exhibited overlapping, broader size distributions with peaks at 25 nm (FWHM = 22, 23, and 23 nm, respectively). This implies two deposition regimes: an early-time regime, where more of the smaller globules are deposited and a second, slightly broader distribution, which stays constant even at long deposition times. We suggest two potential mechanisms that may be responsible for the early time deposition regimes. First, the outer surface of the target, which is ablated during very early times, may not be identical in composition to the remainder of the target, due to a thin film of water vapor that freezes on the target prior to loading. Second, the gradual coalescence of deposited globules could be responsible for the initial increase in globule size with deposition time. The existence of two similar deposition regimes was also confirmed for a second target concentration (0.5 wt. %). The implication of the dual early-time deposition regimes is that it becomes possible to establish a rule of thumb that the globule size distributions resulting from all depositions longer than the critical time are comparable with each other. This is useful when varying other MAPLE deposition parameters, such as target concentration.

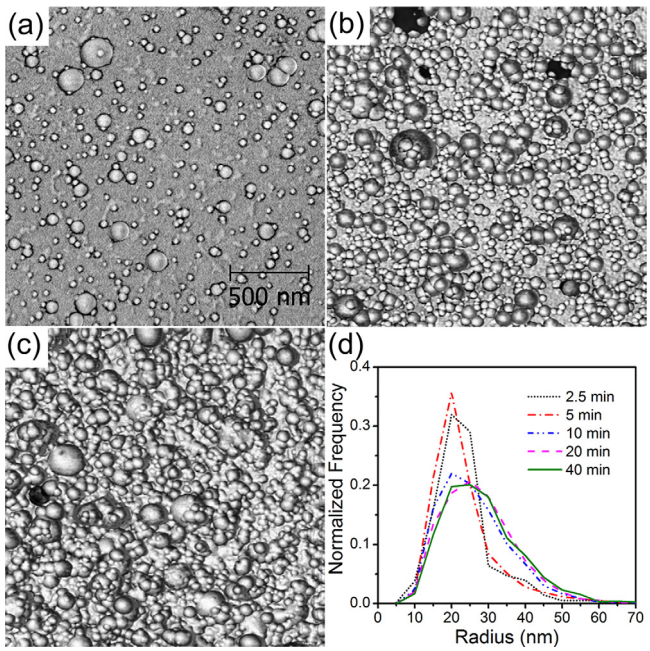

FIG. 1. AFM phase images of PMMA films formed after (a) 2.5 min, (b) 10 min, and (c) 40 min of MAPLE deposition time. (d) Histogram plot of nanoglobule radius for five deposition times.

The effect of polymer target concentration on the nanostructure was then examined, with concentrations ranging over more than an order of magnitude. The nanoglobule size distributions of the resulting films were analyzed similarly to above. All four target concentrations are significantly below the polymer overlap concentration, $C^* \approx 0.06$, for 15 kg/mol PMMA in good solvent, where the overlap concentration is the volume fraction at which polymer molecules in the solution begin to overlap each other.[17] The deposition time for each concentration was different as longer times were used for lower polymer concentrations to ensure full coverage of the substrate. However, all deposition times were greater than or equal to 10 min. As discussed above, the nanoglobule

distribution is fully developed for depositions with times above the critical time, thus we are able to equitably compare the nanoglobule size at different target concentrations.

AFM phase images of MAPLE deposited films for the four concentrations studied are shown in Figs. 2(a)–2(d). Larger globules, which were not present in the images of films with target concentrations of 0.05% (Fig. 2(a)) and 0.1% (Fig. 2(b)), began to appear in the film deposited from 0.5% (Fig. 2(c)) target concentration. Large globules were present in greater numbers in the film deposited from 1% (Fig. 2(d)) target concentration. A histogram of the nanoglobule size distribution is provided in Fig. 2(e). The selective presence of large globules in higher concentration depositions was quantitatively confirmed by the histogram analysis. The tail of the globule distribution curves (right side) increases in magnitude and length with increasing concentration. The increasing number of large globules in higher concentration depositions is also evident in another statistic: the normalized area which is occupied by globules with a radius of 50 nm or more, A_{50} ($A_{50} = A_{large}/A_{occupied}$ where A_{large} is the total area occupied by globules of radius 50 nm or greater and $A_{occupied}$ is the total area occupied by globules of all sizes). In agreement with histogram data, the values of A_{50} are similar for 0.05% and 0.1%, at $A_{50} = 0.11$ and 0.092, respectively. The value increases significantly for higher concentrations; $A_{50} = 0.37$ for 0.5% and $A_{50} = 0.70$ for 1% target concentrations. The histogram peak maximum does not change significantly, even over the 20-fold increase in concentration discussed here. The numerical mean of the nanoglobule radii is ~60% higher for 1% target concentration than for 0.05% (increases from 23 nm to 37 nm), and the increase in standard deviation is greater, at ~200% (increases from 10 nm to 31 nm). These results together suggest that the predominant difference between high and low target concentration MAPLE depositions is the presence of larger globules, and not the complete elimination of small globules.

In previous work,[11] we briefly addressed the formation of MAPLE-deposited polymer nanoglobules within the context of the Zhigilei model[18–20] of target ablation in the MAPLE process. Molecular dynamics simulations show that phase explosion causes polymer molecules to be ejected from the MAPLE target within clusters of solvent. We proposed that the observed polymer nanoglobules originate when the solvent evaporates from the ejected polymer-solvent clusters during flight from target to substrate. Zhigilei and coworkers also directly addressed the issue of the size of ejected clusters by simulation,[20] as well as the mass of experimentally observed surface features on MAPLE-deposited films.[19] In the simulation work, the size distribution of ejected clusters was characterized as a function of fluence and polymer target concentration, where the size was measured in the number of mers of polymer (N = 100 mers per chain) plus molecules of solvent in each cluster. A power law dependence of $N^{-1.4}$ was identified. However, due to computational limitations,[20] the cluster sizes considered in the work were orders of magnitude smaller than those in actual MAPLE experiments. In a complementary experimental study,[19] scanning electron microscopy was used to estimate the size of micron-scale deposited features, and the polymer density was used to obtain the features' masses. The relationship between cluster mass and normalized yield was again fit by a power law, here with an exponent of $N^{-1.6}$.

In Fig. 3(a), the size distribution data for films deposited from 0.05 and 0.1 wt. % solutions is plotted with 95% confidence intervals. The best power law fit was found for both 0.05 and 0.1 wt. % ($N^{-2.1}$ and $N^{-1.9}$, respectively) over the radius range of 30 nm $\leq R \leq$ 65 nm. An intermediate power law fit with exponent of $N^{-2.0}$ was included in the graph in Fig. 3(a). For globules larger than 65 nm, the number of globules present in each film is inadequate for our analysis to generate meaningful statistics, and thus these were not included in the fit. For globules smaller than 30 nm ($<5 \times 10^5$ mers), the data no longer follow a power law expression. A potential explanation for the deviation from power law behavior is that during deposition, the smallest globules may have been buried underneath larger globules, and thus were not measureable. It is also possible that coalescence of deposited globules into larger features could skew the distribution. We note that for both concentrations, the exponent in the power law fit is more negative than that reported in simulations[20] and experimental[19] measurements. The difference in scaling could potentially be attributed to the large differences in the sizes of the clusters considered. The largest simulated polymer/solvent clusters contain approximately 30 polymer molecules, which would correspond to a radius of ~5 nm if the solvent were removed. The smallest experimentally-measured polymer features[19] are still an order of magnitude larger than those considered in our work.

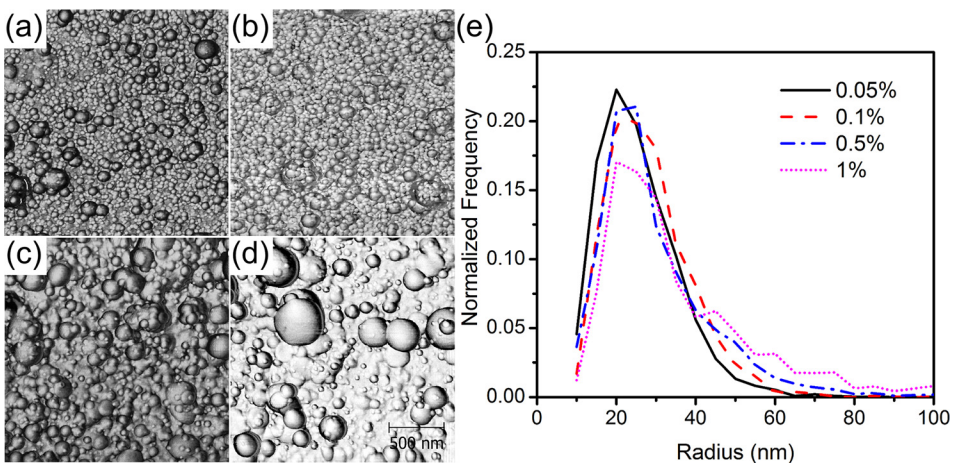

FIG. 2. AFM phase images of PMMA films MAPLE deposited from (a) 0.05%, (b) 0.1%, (c) 0.5%, and (d) 1.0% PMMA by weight target solutions. (e) Histogram plot of nanoglobule radius for four target concentrations.

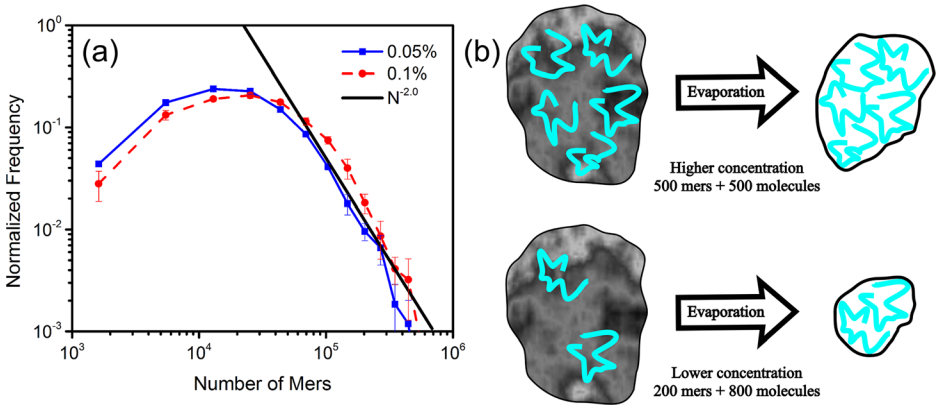

FIG. 3. (a) Histogram plot of number of mers per nanoglobule for 0.05% (dotted red curve) and 0.1% (solid blue curve) MAPLE-deposited films, compared with $N^{-2.0}$ scaling. (b) Schematic of nanoglobule formation from MAPLE-ejected polymer/solvent clusters. Equal sized clusters with different polymer concentrations will form differently sized nanoglobules after evaporation.

In the aforementioned computational study,[20] target concentration was found not to change the size scaling of the ejected clusters, even for targets that contain no polymer. It is important to consider that the size metric for this molecular dynamics simulation is that of mers and solvent molecules together. For different target concentrations, ejected clusters of equal size contain different volume fractions of polymer. After evaporation of the solvent, the clusters can then form differently sized polymer nanoglobules as depicted schematically in Fig. 3(b). The size of the resulting polymer-only clusters would be smaller for the lower concentration case, resulting in decreasing nanoglobule size with decreasing concentration. Accordingly, the volume of the nanoglobules would be expected to vary linearly with concentration with a slope of 1 within this concentration regime. While this suggested mechanism appears adequate for describing globule size distribution for films deposited from higher concentration targets (>0.5%), our results indicate that it does not fully capture the behavior at low concentrations. The influence of target concentration on the linearity of globule size, as well as the critical time will be investigated in detail in future work.

In this work, the origins of nanostructure formation in MAPLE-deposited PMMA coatings were probed via two MAPLE parameters: deposition time and target concentration. Different short and long time deposition time regimes were observed in the nanoglobule size distributions. For depositions less than the critical time, a narrower distribution with a peak at 20 nm radius was found. For longer depositions the distribution was wider and peaked at 25 nm. After the critical time, the size distribution does not change significantly with increasing time, indicating that the size distribution is fully developed. The average size and standard deviation of the nanoglobules both increased with increasing polymer concentration in the MAPLE target. While the peak of the size distribution was similar for all concentrations, the high-radius tail of the distribution became larger with increasing concentration. Our experimental results were compared with Zhigilei's experimental[19] and computational[20] results for MAPLE-deposited clusters. Power law scaling of the globule size was observed, with exponent $N^{-2.0}$. This supports the proposed mechanism of formation of nanostructured MAPLE films, in which ejected clusters of polymer and solvent assemble into polymer nanoglobules during flight from the target to substrate.

We acknowledge support of the National Science Foundation (NSF) Materials Research Science and Engineering Center program through the Princeton Center for Complex Materials (DMR-0819860) and usage of the PRISM Imaging and Analysis Center at Princeton University. R.D.P. acknowledges partial support from the NSF through a CAREER Award (DMR-1053144) and the AFOSR through a YIP Award (FA9550-12-1-0223).

[1]K. B. Shepard and R. D. Priestley, Macromol. Chem. Phys. **214**, 862 (2013).
[2]A. Piqué, Appl. Phys. A **105**, 517 (2011).
[3]A. P. Caricato, M. Cesaria, G. Gigli, A. Loiudice, A. Luches, M. Martino, V. Resta, A. Rizzo, and A. Taurino, Appl. Phys. Lett. **100**, 073306 (2012).
[4]P. Wu, B. Ringeisen, J. Callahan, M. Brooks, D. Bubb, H. Wu, A. Piqué, B. Spargo, R. McGill, and D. Chrisey, Thin Solid Films **398–399**, 607 (2001).
[5]R. Pate, R. McCormick, L. Chen, W. Zhou, and A. Stiff-Roberts, Appl. Phys. A: Mater. Sci. Process. **105**, 555 (2011).
[6]S. Guha, D. Adil, N. B. Ukah, R. K. Gupta, and K. Ghosh, Appl. Phys. **105**, 547 (2011).
[7]F. M. Miroiu, G. Socol, A. Visan, N. Stefan, D. Craciun, V. Craciun, G. Dorcioman, I. N. Mihailescu, L. E. Sima, S. M. Petrescu, A. Andronie, I. Stamatin, S. Moga, and C. Ducu, Mater. Sci. Eng., B **169**, 151 (2010).
[8]R. Cristescu, C. Popescu, G. Socol, A. Visan, I. N. Mihailescu, S. D. Gittard, P. R. Miller, T. N. Martin, R. J. Narayan, A. Andronie, I. Stamatin, and D. B. Chrisey, Appl. Surf. Sci. **257**, 5287 (2011).
[9]C. N. Casey, S. E. Campbell, and U. J. Gibson, Biosens. Bioelectron. **26**, 703 (2010).
[10]F. Sima, E. Axente, C. Ristoscu, I. N. Mihailescu, T. V. Kononenko, I. A. Nagovitsin, G. Chudinova, V. I. Konov, M. Socol, I. Enculescu, L. E. Sima, and S. M. Petrescu, J. Biomed. Mater. Res. Part A **96A**, 384 (2011).
[11]K. B. Shepard, Y. Guo, C. B. Arnold, and R. D. Priestley, Appl. Phys. **110**, 771 (2013).
[12]F. Sima, E. C. Mutlu, M. S. Eroglu, L. E. Sima, N. Serban, C. Ristoscu, S. M. Petrescu, E. T. Oner, and I. N. Mihailescu, Biomacromolecules **12**, 2251 (2011).
[13]R. Cristescu, A. Doraiswamy, G. Socol, S. Grigorescu, E. Axente, D. Mihaiescu, A. Moldovan, R. J. Narayan, I. Stamatin, I. N. Mihailescu, B. J. Chisholm, and D. B. Chrisey, Appl. Surf. Sci. **253**, 6476 (2007).
[14]Y. Guo, A. Morozov, D. Schneider, J. W. Chung, C. Zhang, M. Waldmann, N. Yao, G. Fytas, C. B. Arnold, and R. D. Priestley, Nature Mater. **11**, 337 (2012).
[15]D. Nečas and P. Klapetek, Cent. Eur. J. Phys. **10**, 181 (2012).
[16]C. A. Schneider, W. S. Rasband, and K. W. Eliceiri, Nat. Methods **9**, 671 (2012).
[17]M. Rubinstein and R. Colby, *Polymer Physics* (Oxford University Press, New York, 2003).
[18]E. Leveugle, L. V. Zhigilei, A. Sellinger, and J. M. Fitz-Gerald, J. Phys.: Conf. Ser. **59**, 126 (2007).
[19]E. Leveugle, L. V. Zhigilei, A. Sellinger, and J. M. Fitz-Gerald, Appl. Surf. Sci. **253**, 6456 (2007).
[20]E. Leveugle and L. V. Zhigilei, J. Appl. Phys. **102**, 074914 (2007).